J. Mater. Environ. Sci. 7 (7) (2016) 2453-2467
ISSN : 2028-2508
CODEN: JMESC

Alstonia Scholaris bark as an environmentally benign corrosion inhibitor for Aluminium alloy in sodium hydroxide solution

Namrata Chaubey[1], Vinod Kumar Singh[1], M. A. Quraishi*[2]

[1]*Department of Chemistry, Udai Pratap Autonomous College, Varanasi-221002, India*
[2]*Department of Chemistry, Indian Institute of Technology (Banaras Hindu University), Varanasi-221005, India.*

Received 02 Feb 2015, Revised 21 Aug 2015, Accepted 22 Aug 2015
**Corresponding author: E-mail: maquraishi.apc@itbhu.ac.in ; maquraishi@rediffmail.com*
Ph.no. +91-9307025126; Fax: +91- 542- 2368428

Abstract

Inhibition effect of aqueous extract of Alstonia Scholaris bark (ASB) on the corrosion of aluminium alloy (AA) in 1M NaOH was carried out using gravimetric, electrochemical impedance spectroscopy (EIS), Potentiodynamic polarization (PDP) and linear polarization resistance (LPR) techniques. ASB showed maximum inhibition efficiency (η %) of 92.6% at 2.0 g/L. The adsorption of inhibitor molecules on AA surface obeyed the Langmuir's adsorption isotherm. Tafel Polarization study showed mixed mode of corrosion inhibition of inhibitor. The effective protection of AA in inhibited system was investigated using scanning electron microscopy (SEM) and atomic force microscopy (AFM).

Keywords: Aluminium; AFM; EIS; Polarization; Alkaline corrosion

1. Introduction

Aluminium and its alloys are extremely diverse materials due to their unusual combinations of properties. These materials find their way into broad applications in the various industries such as automotive, aerospace, construction and electrical power generation. Aluminium, with high energy density (8.1 $kWhkg^{-1}$) and an electrode potential of 2.35 V *vs.* standard hydrogen electrode (SHE) in alkaline medium, has emerged as one of the most promising anode materials in Al-air cells [1]. These cells often utilize aluminium alkaline solution systems in which inherent dissolution of metal occurs. The battery performance is determined by the electrochemical and corrosion properties of aluminum anodes [2]. However, aluminium is highly resistant to most acidic and neutral solutions due to the formation of a protective oxide film on its surface. In oxidizing environments the formation of film is very rapid and attack on the metal is negligible [3] but this protective film destroys, when it is exposed to alkaline conditions and corrosion of aluminium occurs, yielding AlO_2^- (aluminate) ions in the alkaline medium**.** In efforts to mitigate aluminium corrosion, the main tactic is to separate the metal from corrosive environments. This can be achieved using corrosion inhibitors.

In literature, a number of organic compounds have been used as effective inhibitors for various metals in corrosive media [4-9] but most of them are synthetic chemicals, expensive and toxic to the environment. In view of this, it is necessary to develop a very cheap and environmentally safe research to diminish self-corrosion rate of aluminium in alkaline medium. In order to achieve the goal, extracts of various parts of plants (leaves, stems, barks, fruits etc) have been used as corrosion inhibitors [10-12] because they are incredibly rich source of naturally synthesized organic compounds that can be extracted using simpler techniques with low cost. In addition, Plant extracts are environmentally acceptable, readily available and renewable source for a wide range of needed inhibitors. We therefore aim to investigate the corrosion inhibition study of aqueous extract of bark of Alstonia Scholaris tree on AA in alkaline media.

Alstonia Scholaris tree belongs to the family Apocynaceae, grows throughout the India, in deciduous and evergreen forests and also in plains [13]. In present study, we are focused on the corrosion inhibition performance of aqueous extract of ASB on AA in 1 M NaOH solution. The inhibiting study was conducted by weight loss measurement, potentiodynamic polarization, linear polarization resistance and electrochemical impedance spectroscopy.

2. Experimental

2.1. Specimen and test solution

Aluminium alloy coupons were purchased from the market and analyzed it in department of Metallurgical Engineering, IIT (BHU). The analysis of result showed that AA specimen having the composition (*wt* %) Si = 0.77, Fe=0.93, Cu=0.02, Mn=0.11, Mg=0.01, Zn=0.01, Cr=0.05, Ti=0.02, V=0.01, Ga=0.01, Al= balance, was used in this study. Stock solution of 1 M NaOH was prepared by dissolving 40 g of solid NaOH in double distilled water.

2.2. Preparation of inhibitor solution

Barks of *Alstonia Scholaris* tree were collected from the campus of Banaras Hindu University, India. Barks were dried in a laboratory oven at 45° C, and ground to powdered form. 1 g of the powder was added to 500 ml of 1M NaOH solution in a round bottom flask and refluxed for 1h. Thereafter, the mixture was cooled and filtered. The precipitate was dried and weighed to confirm the amount of soluble materials present in the solvent. The extract was concentrated by solvent evaporation and maintained up to concentration of 2000 mg/L and used as stock solution. Bark extract test solutions were prepared at concentrations of 0.5, 1.0, 1.5 and 2.0 g/L.

2.3. Inhibitor constituents

ASB contains naturally occurring compounds such as alkaloids flavonoids, and terpenoids [14-16]. The constituent alkaloids include alstonidine, alstonine, chlorogenic acid, chlorogenine, ditain, echitamine, and echitenin, while the triterpenoids include lupeol linoleate and lupeol [17-19]. But two water soluble major constituents obtained from ASB are echitamine and loganin are reported. Because of the presence of heteroatoms, functional group and π-electrons, corrosion inhibition by aqueous ASB extracts can be regarded as synergistic process.

Table 1: Molecular structure of major constituents present in ASB extract

Inhibitor	Major constituents'	Molecular structure	Ref.
ASB	Loganine		[48]
	Echitamine		

2.4. Gravimetric measurement

AA with the dimension of 2.5 × 2.0 × 0.046 cm was used in the weight loss experiment in 1M NaOH solution without and with the addition of different concentrations of bark extract. The AA coupons were abraded with silicon carbide papers with grade of 600, 800 and 1000, degreased with acetone and dried at room temperature. After weighing,

every coupon was placed in the stock solution of 1 M NaOH for 3 hour at 303 K. After the time period, the sample was taken out from the weight loss chamber, washed with distilled water and cleaned with acetone, dried and weighed. The same process was repeated at the temperature range from 313- 333 K.

The corrosion rate of aluminium and inhibition efficiency (η %) were calculated using the following relation [20] **:**

$$C_R = \frac{K \times W}{A \times T \times D} \quad (1)$$

Where K is constant (87.6×10^4), T is the exposure time in hours (h), A is the area of a coupon in cm^2, W is the weight loss (mg) and D is the density of AA in g/cm^3

$$\eta\% = \frac{w_o - w_i}{w_o} \times 100 \quad (2)$$

Where, w_0 and w_i are the weight loss value in the absence and presence of inhibitor, respectively.

2.5. Electrochemical experiment

The electrochemical measurement was carried out by using three electrode cell assembly connected to the Gamry Potentiostat /Galvanostat (Model 300) at room temperature. AA with 1 cm^2 area was used as a working electrode. A platinum foil and a saturated calomel electrode (SCE) i.e. (Cl^-| (4M) Hg_2Cl_2 (s)| Hg (l) | Pt) were used as counter and reference electrodes respectively. Echem Analyst version 5.0 software packages were used for analyzing the electrochemical data. All the tests were performed after 15 minute immersion of AA in the absence and presence of optimum concentration of inhibitors in1M NaOH solution. Before starting impedance experiments, the electrode were allowed to corrode freely and its open circuit potential (OCP) was recorded as a function of time for 200 s to obtain steady state OCP which corresponds to corrosion potential. Impedance measurements were carried out in the frequency range 100 kHz -0.01 Hz using AC signals of amplitude 10 mV peak to peak at open circuit potential.

Linear polarization resistance (LPR) measurements were performed in a potential range - 0.02 V to + 0.02 V vs. with respect to OCP at a scan rate of 0.125 mV/s. Finally, potentiodynamic polarization curves were obtained by shifting the electrode potential automatically from -250 upto + 250 mV_{SCE} vs. OCP at a scan rate of 1 mV/s. the anodic and cathodic curves of the linear Tafel plots was extrapolated to obtain corrosion current densities (I_{corr}).

2.6. Surface analysis

AA coupons of size 2 × 2.5 × 0.046 cm were immersed in 1 M NaOH in absence and presence of ASB for 3 h at 303 K. Thereafter, the metal specimens were taken out, washed with distilled water, degreased with acetone, dried at ambient temperature, and mechanically cut into 1 cm^2 sizes for SEM and AFM investigations.

The SEM of the AA surface was performed at an accelerating voltage of 5000 V and 5KX magnification using FEI Quanta 200F microscope. The AFM was performed using NT-MDT multimode, Russia, controlled by solver scanning probe microscope controller. The inhibited system contains optimum concentration (2.0 g/L) of ASB extract.

3. Result and discussion

3.1. Gravimetric test

3.1.1. Effect of inhibitor concentration

The effect of addition of different concentration of ASB extract on the AA in 1 M NaOH solution was studied by weight loss measurement at 303 K after 3 hour immersion. The values of inhibition efficiency (η %) and corrosion rate (C_R) are summarized in Table 2. The result showed that the inhibition efficiency increases and corrosion rate decreases as the concentration of the inhibitor increases from 0.5 to 2.0 g/L. The highest η % and lowest C_R of metal were obtained at optimum concentration (2.0 g/L). Insignificant change in η % was noticed above 2.0 g/L (optimum concentration).

Table 2: Inhibition efficiency (η %) and corrosion rate (C_R) values obtained from gravimetric measurement for AA in 1M NaOH containing various concentrations of the inhibitor at 303K.

Inhibitors	C_{inh} **(g/L)**	C_R **(mm/year)**	θ	η **(%)**
Blank	0.0	351.0	-	-
ASB	0.5	75.7	0.67	67.8
	1.0	62.7	0.73	73.3
	1.5	32.4	0.86	86.2
	2.0	17.3	0.92	92.6

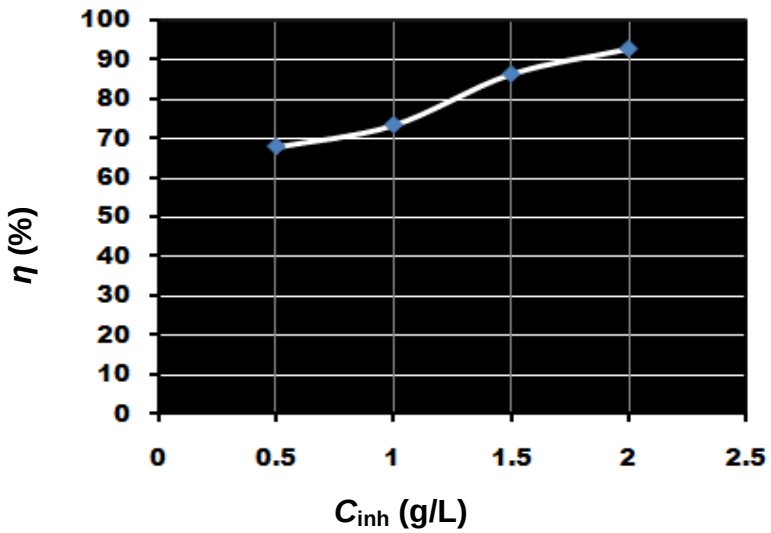

Figure 1: Effect of concentration on inhibition efficiency

3.1.2. Solution temperature

Weight loss experiments were also carried out at different temperatures (303- 338 K) on corrosion behaviour of AA in the absence and presence of ASB extract for 3 h immersion in 1M NaOH. The corresponding inhibition efficiency (η %) with increasing temperature is shown in Figure 2

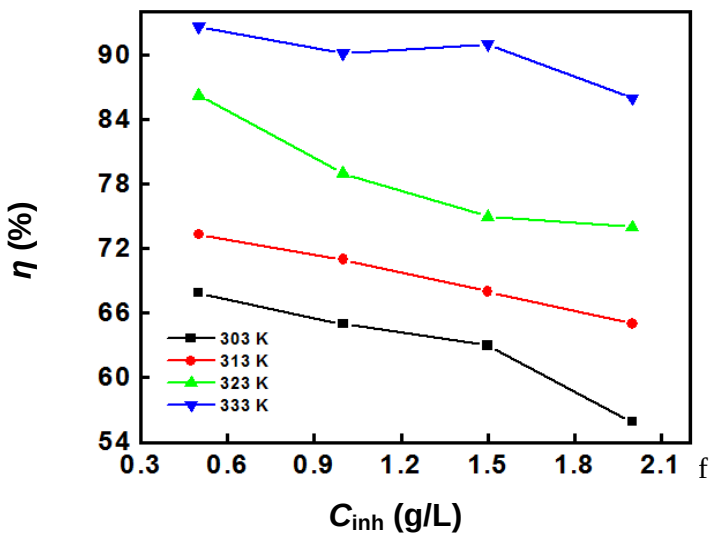

f

Figure 2: Inhibition efficiency at different concentrations of ASB extract at different temperatures

As shown in Figure 2, corrosion rate (C_R) increases and inhibition efficiency (η %) decreases with rise in temperature and this increase in corrosion rate may be due to an appreciable decrease in the adsorption of the inhibitor molecules on the AA surface with increasing temperature.

With decrease in adsorption, more desorption of inhibitor molecules occur because these two opposite processes are in equilibrium. Due to more desorption of inhibitor molecules at higher temperatures, the larger surface area of AA are affected with alkali environment, resulting in increased corrosion rates and decreased η % with increase in temperature. To calculate the apparent activation energy (E_a) for corrosion process Arrhenius Eq. (3) was used:

$$\log C_R = \frac{-E_a}{2.303RT} + \lambda \qquad (3)$$

where, E_a is the apparent activation energy of the corrosion process, R is the general gas constant, and A is the Arrhenius pre-exponential factor.

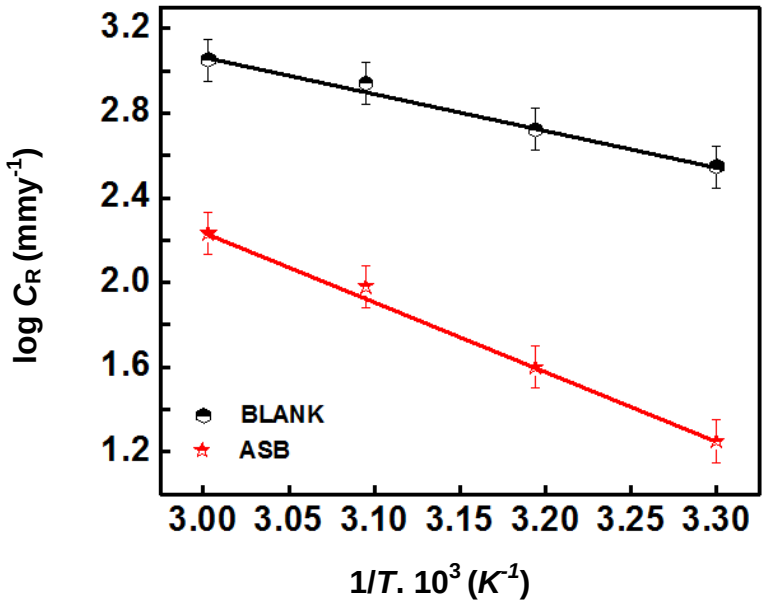

Figure 3: Arrhenius plots for AA corrosion rates (C_R) in 1M NaOH without and with optimum concentration of ASB extract.

The E_a values were determined by linear regression between log C_R and 1/T (Figure 3). The E_a value for inhibited system is higher (55 kJmol^{-1}) than that of uninhibited system (33.6 kJmol^{-1}). The higher value of E_a indicates that more energy barrier for the corrosion reaction in presence of the inhibitor is attained. Thus the adsorbed inhibitor molecules prevent charge or mass transfer from the metal surface [21].

3.1.3. Adsorption isotherm

Basic information of the interaction of inhibitor molecules to the metal surface could be provided from the adsorption isotherms. To determine the adsorption process, the surface coverage (θ) values corresponding to various concentrations of inhibitors have been used to explain the correct isotherm [22].

The surface coverage values (θ) for different inhibitor concentration were tested by fitting to various isotherms such as Freundlich, Temkin, Langmuir and Frumkin isotherms. Among these isotherms, Langmuir adsorption isotherm was best fitted (Figure 4) and can be given by following equation [23]:

$$\frac{C_{\text{inh}}}{\theta} = \frac{1}{K_{\text{ads}}} + C_{\text{inh}} \qquad (4)$$

where K_{ads} is the adsorption equilibrium constant, C denotes the concentration of the inhibitor and θ is surface coverage value. The plot of log C_{inh}/θ vs. C_{inh} gave a straight line as shown in Figure 4, which indicates

that the adsorption of inhibitor molecules on the metal surface obeys Langmuir adsorption isotherm. On the other hand, the equilibrium constant of adsorption (K_{ads}) is also related to standard energy of adsorption (ΔG^0_{ads}) by the equation [24]:

$$K_{ads} = \frac{1}{C_{(sol.)}} \exp\left(\frac{\Delta G^0_{ads}}{RT}\right) \quad (5)$$

where R is universal gas constant, T is the absolute temperature (K) and C is the concentration of water (1000 g/L). The values of K_{ads} is representing here in $g^{-1}L$, thus in this equation, the concentration of water is taken in gL^{-1} (1000 gL^{-1}) in the place of 55.5 mole/L.

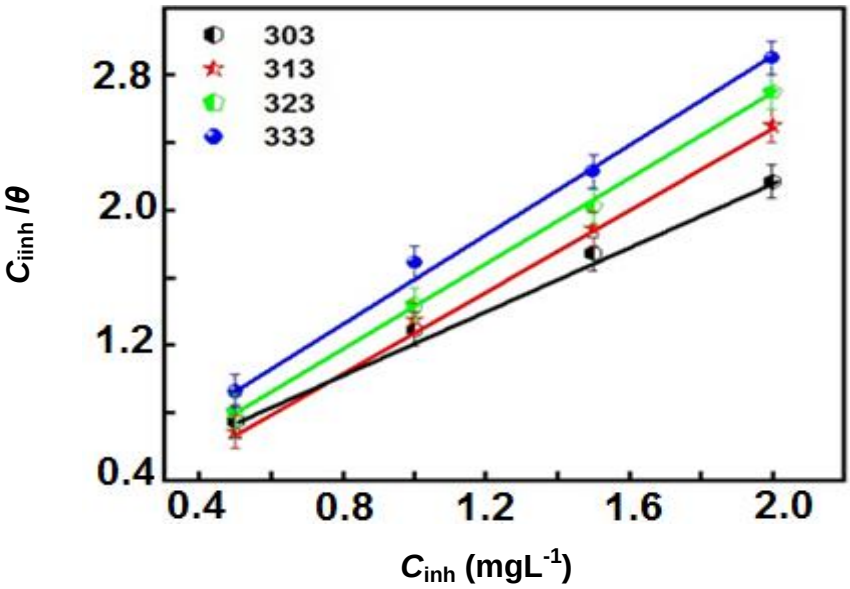

Figure 4: Langmuir isotherm plots for adsorption of inhibitor on AA in 1M NaOH.

The observed values of K_{ads} and ΔG_{ads} are given in Table 3.

Table 3: Thermodynamic parameters obtained for adsorption of inhibitor on AA in 1 M NaOH at different temperatures.

Inhibitor	Temperature	K_{ads} $10^3(g^{-1})$	G^o_{ads} $(KJmol^{-1})$
ASB	303	5.75	-21.81
	313	3.66	-21.35
	323	1.88	-20.24
	333	1.77	-20.70

The obtained values of ΔG^0_{ads} show the regular dependence on temperature, indicating a good correlation among thermodynamic parameters. The large negative values of ΔG^0_{ads} ensure the spontaneity of the adsorption process and the stability of the adsorbed layer on the metal surface [25, 26] as well as a strong interaction between the inhibitor molecules and the aluminium metal surface [27].

Generally, absolute values of ΔG^0_{ads} up to -20 kJ mol^{-1} are consistent with physisorption, while those around -40 kJ mol^{-1} or higher are associated with chemisorption as a result of the sharing or transfer of electrons from organic molecules to the metal surface to form a coordinate type of metal bonds [28]. Here, the calculated ΔG^0_{ads} values are ranging between 20.24 – 21.81 kJ mol^{-1} indicating that the adsorption mechanism of ASB extract on aluminium metal in 1M NaOH solution at the studied temperatures is mainly physical adsorption [29].

3.2. Electrochemical measurement

3.2.1. Electrochemical impedance spectroscopy

Impedance spectra for AA in 1M NaOH solution in the absence and presence of different concentration of inhibitor are recorded and displayed in the form of Nyquist plot (Figure 5). This plot shows depressed semicircles of identical shape in uninhibited and inhibited systems indicating that the presence of ASB extract increases the impedance but does not change the other aspects of corrosion mechanism occurred due to their addition**.** The diameter of the semicircle in the case of uninhibited solution is much smaller but by the addition of inhibitor, it increases with increasing concentration. The maximum impedance modulus is obtained at optimum concentration (2.0 g/L). Impedance diagram contains three times constant which are noticed for AA in alkaline solution namely: a capacitive time constant at higher frequencies, an inductive time constant at medium frequencies and a second time constant at low frequencies value. Similar results have been given in the literature for the corrosion of pure aluminum in alkaline solutions [30-32]. The appearance of the inductive loop is the characteristic feature of these impedance spectra. It should be noticed that these loops are not in perfect semicircles (but in depressed semicircles) and such behavior may be due to the frequency dispersion, surface heterogeneity and rough-textured metal surface. It can be observed that the diameter of the semicircles increases with increase in concentrations of ASB extract, indicating that corrosion is mainly a charge transfer controlled process.

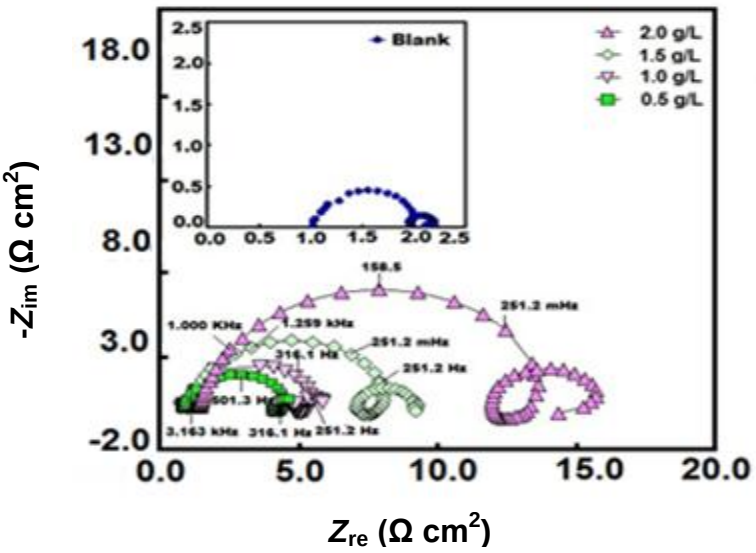

Figure 5: Nyquist plots of AA in 1M NaOH without and with different concentrations of ASB extract at 303K

First time constant at higher frequencies can be explained by the charge transfer of the corrosion process and to the formation of protective (oxide) layer [33]. According to Brett, [34-35] the first time constant is involved in the reaction of aluminum oxidation at the metal/oxide/electrolyte interface. This process explains the formation of Al^{+} ions at the metal/oxide interface and their migration through the oxide layer due to high electric field strength to the oxide/solution interface where they are oxidized to Al^{3+}. At the oxide/solution interface, OH^{-} or O^{2-} ions are also formed. The inductive loop observed at intermediate frequency may be attributed to the relaxation process in oxide presents on the electrode surface obtained by adsorbed species as OH^{-}_{ads} [36]. Some researchers emphasized on surface roughening because the shifting of inductive loop approaches towards higher frequencies is dependent on hydroxide ion concentration. It can be explained by the fact that due to increasing hydroxide ion concentration, the anhydrous film becomes thinner, the pore diameters widens and the hydrated layer thicker due to the presence of extensive amount of aluminates and hydroxide species in the solution. Because of the widening of the pore diameter and thinning of the anhydrous film, the chemical and electrochemical dissolution process proceed easily resulting in surface roughening. The inductive

loop shifts towards higher frequencies with increasing potential in the positive direction can be attributed to the increasing movement rate of aluminum and hydroxide species and to the enlargement of pores resulting in surface roughening [37]. Second capacitive loop at lower frequency values arise because of the metal dissolution.

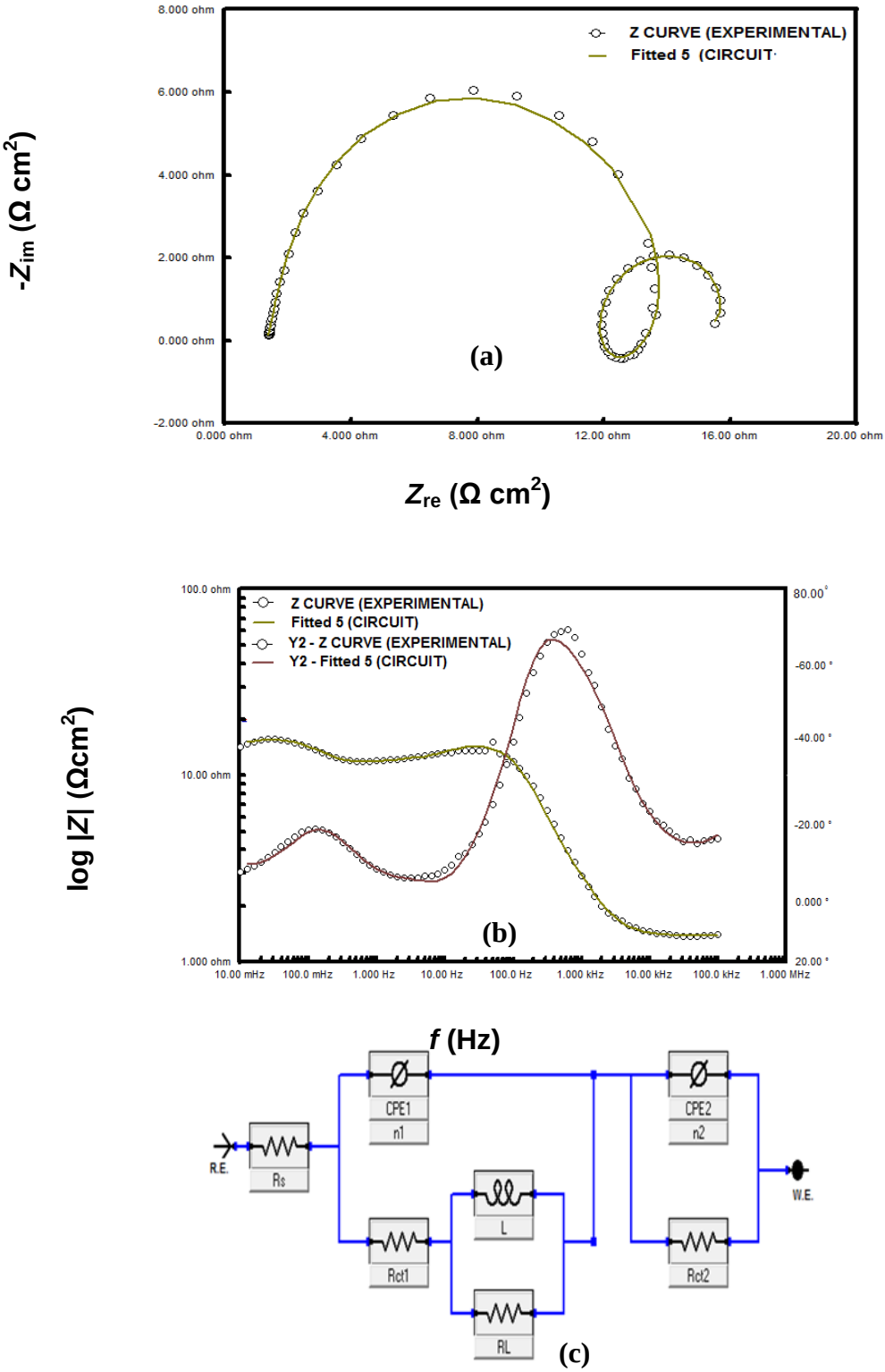

Figure 6: Simulated and experimentally generated EIS plots (a) Nyquist plot (b) Bode phase angle (c) Electrical equivalent circuit used for the analysis of impedance spectra

Table 4: Electrochemical impedance parameters for AA in 1 M NaOH in the absence and presence of different concentrations of inhibitor.

Inhibitor (g/L)	R_s (Ω)	Q_1 ($S\Omega^{-1}cm^2$)	n_1	$(R_{ct})_1$ (Ωcm^2)	L (Hcm^2)	R_L (Ωc^2)	Q_2 ($S\Omega^{-1}cm^2$)	n_2	$(R_{ct})_2$ (Ω cm^2)	C_{dl} (μF cm^{-2})	η (%)
Blank	1.023	500×10^{-6}	0.975	0.849	0.221	0.121	39.8×10^{-6}	0.521	0.188	413.08	--
0.5	0.741	63.18×10^{-6}	0.886	2.745	0.154	1.143	38.8×10^{-6}	0.780	0.200	122.3	71.4
1.0	0.824	43.65×10^{-6}	0.924	6.985	0.184	0.281	37.4×10^{-6}	0.703	1.229	102.31	87.6
1.5	0.915	54.78×10^{-6}	0.982	7.469	0.114	1.770	33.2×10^{-6}	0.757	0.886	78.51	87.9
2.0	1.020	65.64×10^{-6}	0.989	13.83	0.078	3.078	$19.5e\times10^{-6}$	0. 881	0.638	41.79	93.05

All the impedance parameters were calculated (Table. 4) by the use of the equivalent circuit model as shown in Figure 6c**.** The circuit contains R_s (the resistance of solution between working electrode and counter electrode), C_{dl} in parallel to the R_{ct}, and R_{ct} in series with the parallel inductive elements L and R_L. In the Impedance spectra the existence of L in the presence of ASB extract indicated that aluminium is still dissolved by the direct charge transfer at the inhibitor adsorbed electrode surface [38].

The explanation for the presence of double layer capacitance is in parallel with the impedance is due to the charge transfer reaction. The constant phase element (*CPE*) is introduced in the circuit rather than a pure double layer capacitance to fit the semicircle more accurately. The impedance for *CPE* (Z_{CPE}) is expressed as:

$$Z_{CPE} = \left(\frac{1}{Q}\right)\left[(j\omega)_n\right]^{-1} \quad (6)$$

Where, Q the proportionality constant comparable to capacitance, j is the imaginary unit and ω is the angular frequency ($\omega = 2\pi f$, f is the frequency at maximum in Hz), n is the phase shift which related to degree of surface non-homogeneity. Depending on n, *CPE* can represent resistance ($Y_0 = R$, n = 0), capacitance ($Y_0 = C$, $n = 1$), inductance ($Y_0 = L$, $n = -1$) or Warburg impedance ($n = 0.5$, Y_0 =W). Analysis of Table. 4 reveals the R_{ct} values in the presence of inhibitor are more than in uninhibited system. The maximum R_{ct} values are found in optimum concentration (2.0 g/L) of ASB extract and the increase in values for inhibited system attributed to the decrease in the active surface necessary for the corrosion reaction. The inhibition efficiency associated with charge transfer resistance values is calculated by following equation:

$$\%IE = \frac{R_{p(inh)}^{-1} - R_p^{-1}}{R_{p(inh)}^{-1}} \times 100 \quad (7)$$

Where R_p^{-1} and $R_{p(inh)}^{-1}$ are the polarization resistance values without and with inhibitor, respectively.

The value of double layer capacitance (C_{dl}) decreases with increasing inhibitor concentration. The double layer between the electrolyte and charged metal surface is considered as an electrical capacitor. The adsorption of ASB on aluminium surface decreases its electrical capacity because they displace water molecules and other ions originally adsorbed on the surface. The decrease in capacitance of an inhibited system may be imputed to the formation of a protective layer on the electrode surface [39]. The double layer capacitance (C_{dl}) values were calculated using the following equation:

$$C_{dl} = Q(\omega_{max})^{n-1} \quad (8)$$

where ω_{max} is the angular frequency at which imaginary element reaches a maximum. Moreover, Addition of inhibitors increases the values of n that explains reduction of surface inhomogeneity due to the adsorption of inhibitor molecules on the most active adsorption sites at the AA surface [40].

Indeed, the lower *n* value for uninhibited solution (n = 0.975) describes an inhomogeneity in surface occurring from surface metal roughening and/or surface of corrosion products. The values of *n* lies between 0.886 and 0.989 in the case of inhibited solutions.

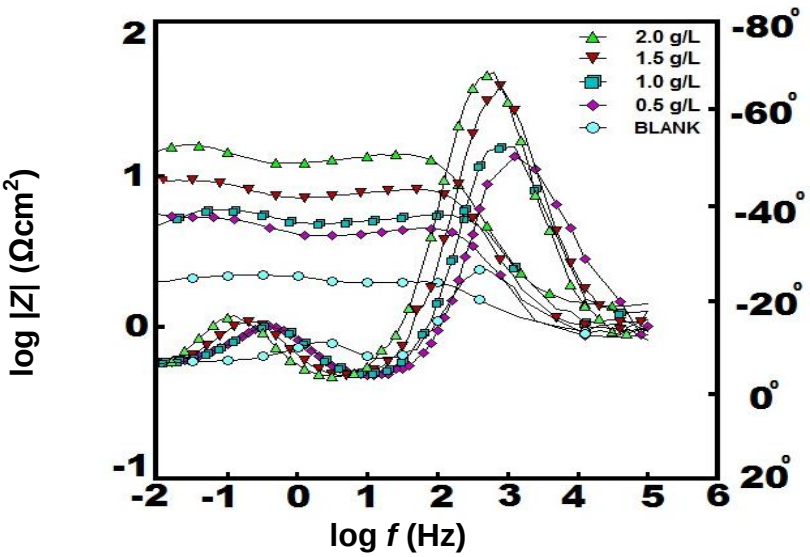

Figure 7. Bode plots and phase angle plots of AA in 1M NaOH without and with different concentration of inhibitor at 303 K

The Bode impedance modulus and phase angle plots recorded for AA electrode immersed in 1M NaOH in the absence and presence of different concentrations of ASB at its OPC are given in Figure 7. The impedance plots at higher frequency limit (100 kHz) correspond to the ohmic resistance of the films of corrosion product and the solution between the working electrode and reference electrode.

At high frequency the values of log |Z| and phase angle falls to zero. This indicates the resistive behavior of metal electrode which corresponds to solution resistance enclosed between the reference and working electrodes [41]. In the intermediate frequency region, a linear relationship between log |Z| vs. log f with a slope near -1 and the phase angle approaching 80^0 has been observed. For an ideal capacitor, the value of S and α° should be -1 and -90 $^{\circ}$ respectively. However, in this case, the maximum slope value reaches up to -0.81 and maximum phase angle was 72^0. These deviations considered to be the deviation from the ideal capacitive behavior at intermediate frequencies [42].

3.2.2. Potentiodynamic polarization study

The effect of ASB extract on the corrosion reactions was also determined by potentiodynamic polarization techniques. After adding inhibitor, the changes observed in the polarization curves are usually used as criteria to classify inhibitors as cathodic, anodic or mixed [43, 44]. Tafel polarization curves for aluminium metal in 1 M NaOH at different concentrations of ASB are displayed in Figure 8. It can be observed from the curves that the presence of inhibitor causes a prominent decrease in corrosion rate, i.e. shifts the anodic curves to more positive potentials and cathodic curves to more negative potentials and to the lower values of corrosion current densities. The linear section of cathodic and anodic Tafel plots is extrapolated to the corrosion potential in order to get polarization parameters for corrosion of AA in 1M NaOH without and with additives. From the figure, it is revealed that the addition of inhibitors shifts the cathodic and anodic branches toward lower currents, probably as a consequence of the blocking effect of the adsorbed inhibitor molecules. The polarization parameters such as corrosion potential (E_{corr}), anodic and cathodic Tafel slopes (β_a and β_c), corrosion current density (I_{corr}), polarization resistance (R_p) and inhibition efficiency (η %) values are shown in Table 5.
The η % using values of I_{corr} and R_p were calculated by following equation:

$$\eta\% = \frac{I^0_{corr} - I_{corr}}{I^0_{corr}} \times 100 \quad (9)$$

where I^0_{corr} and I_{corr} are the corrosion current density without and with inhibitor. It can be observed that the corrosion rate and corrosion current density (I_{corr}) noticeably decreases in presence of inhibitor, which suggests that the rate of electrochemical reaction was retarded due to formation of a protective film of inhibitor on metal surface and this protective film created a barrier between metal and corrosive medium.

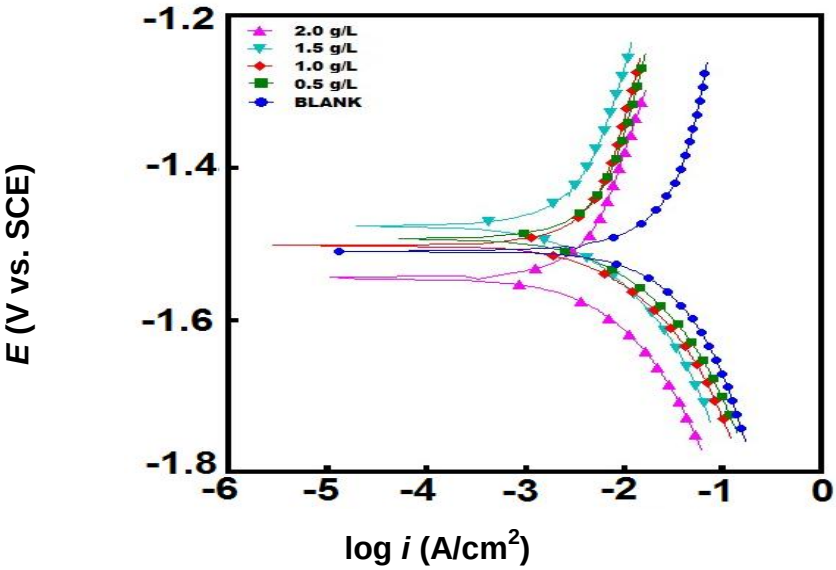

Figure 8: Potentiodynamic polarization curves of AA in 1M NaOH without and with different concentration of ASB extract at 303 K

No effective change was observed in the corrosion potential (E_{corr}) value with respect to the blank. Both anodic and cathodic polarizations are influenced simultaneously, almost to the same extent, which indicate the influence of ASB on both the anodic and the cathodic reactions; hydrogen evolution and metal dissolution. If the displacement in corrosion potential is more than 0.085 V with respect to corrosion potential of the blank, the inhibitor can be seen as a cathodic or anodic type [45]. However, in the present case, the maximum displacement occurs in E_{corr} is 0.024 V which is much less than 0.085 V, suggesting mixed mode of inhibitors.

Table 5: Tafel polarization parameters for AA in 1 M NaOH in the absence and presence of different concentrations of inhibitor at 303 K.

Inhibitor	**Tafel polarization**					
	I_{corr} (mAcm^{-2})	E_{corr} (V/SCE)	β_a (V/dec)	β_c (V/dec)	C_R (mpy×10^3)	η (%)
Blank	96.3	-1.508	1.001	0.504	41.3	--
0.5 g/L	23.05	-1.490	0.703	0.151	5.99	83.33
1.0g/L	11.47	-1.500	1.922	0.162	3.63	88.16
1.5g/L	10.36	-1.473	2.342	0.169	3.16	89.30
2.0g/L	4.31	-1.480	1.715	0.159	1.85	95.53

3.2.3 Linear polarization resistance

Linear polarization resistance (R_p) values were obtained from the resulting plot of current density versus potential. From the measured polarization resistance values, the η % has been calculated using the relation:

$$\eta\% = \frac{R_{p(inh)} - R_p}{R_p} \times 100 \quad (10)$$

where R_p and $R_{p\,(inh)}$ is polarization resistance in the absence and presence of inhibitors. The calculated values of R_p in 1 M NaOH solution with the different concentration of extracts are shown in Table 6. The linear polarization resistance value (R_P) is higher in the inhibited system as compared to the blank that means lowering of corrosion rate occur due to presence of ASB. The maximum value is observed at the optimum concentration (2.0 g/L) of ASB, suggesting the formation of its adherent protective film on aluminium surface.

Table 6: Linear polarization parameters for AA in 1 M NaOH in the absence and presence of different concentrations of inhibitor at 303 K.

Linear polarization	
R_p (Ωcm^{-2})	η (%)
1.279	--
4.50	76.04
8.68	86.04
9.34	87.04
13.57	92.30

3.3. Surface morphology study

3.3.1. Scanning Electron Microscope:

The SEM images of aluminium in the absence and presence of 2.0 g/L inhibitor in 1 M NaOH are displayed in Figure 9 a-b.

Figure 9a shows the roughness of metal surface on which pits and scratches was observed due to strong damaged by the attack of NaOH. After adding 2.0 g/L of ASB extracts, the smoothness of the aluminium surface (Figure 9b) results. The close observation of this micrograph proved that there is less damage of AA surface occurs, which is achieved due to adsorption of inhibitor molecules.

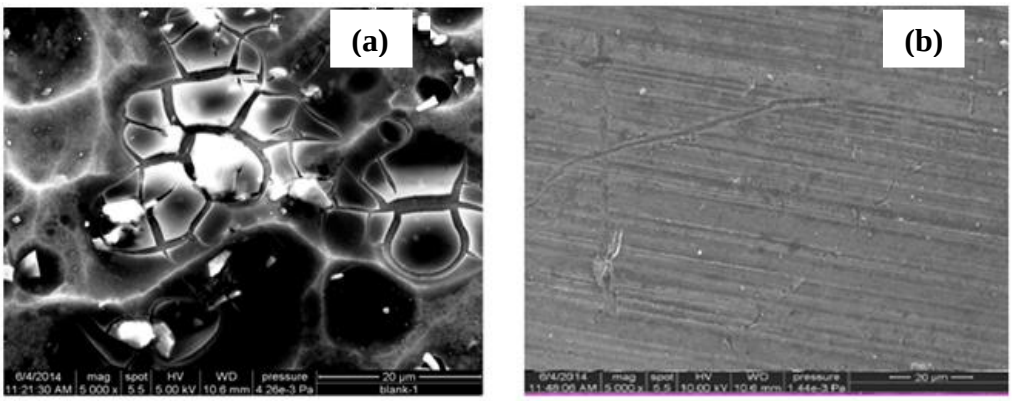

Figure 9: SEM micrographs of (a) uninhibited and (b) inhibited AA sample at 2.0 gL^{-1} of ASB in 1M NaOH

3.3.2. Atomic force Microscope

The three dimensional AFM images are displayed in Figure 10a-b. Figure 10a shows the image detected in 1 M NaOH solution. As can be seen in figure, aluminium surface shows much more damages after exposing it on 1M NaOH and the roughness of surface height is measured as 800 nm. Figure 10b displays the AFM image of surface in inhibited system. The surface height is reduced from 800 nm to 200 nm after adding 2.0 g/L of ASB extract indicated the formation of protective layer on it.

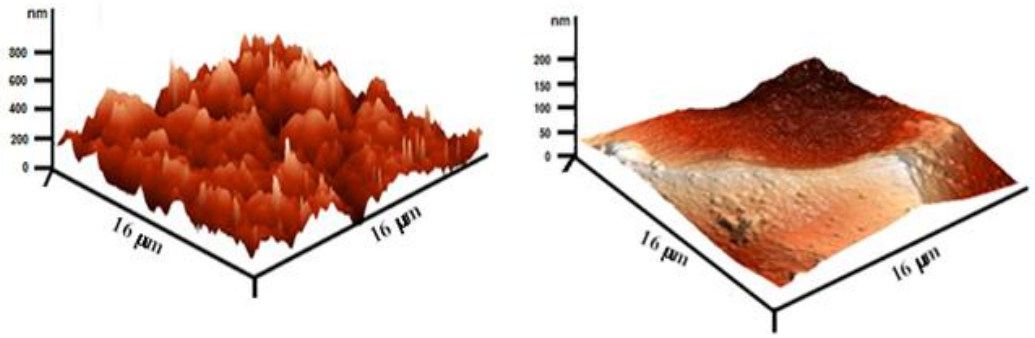

Figure 10: AFM three dimensional images of (a) uninhibited (b) inhibited AA sample containing 2.0 g/L of ASB extract in 1M NaOH

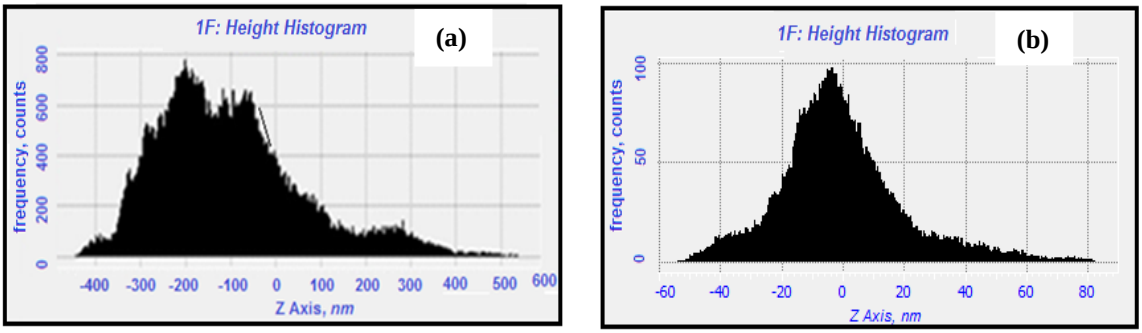

Figure 11: Height profile diagram (a) uninhibited (b) inhibited AA sample immersed in 2.0 gL^{-1} of ASB in 1M NaOH

Figure 11a-b illustrates height profile diagram which are made along the lines marked in corresponding Figure 10a-b. AFM image techniques were used to obtain the root-mean-square roughness, Rq (the average of the measured height deviations taken within the evaluation length and measured from the mean line), average roughness, Ra (the average deviation of all points roughness profile from a mean line over the evaluation length), and the maximum peak-to-valley (P-V) height values (largest single peak-to-valley height in five adjoining sampling heights). The obtained values of the average roughness (Ra), rms roughness (Rq) maximum peak-to-valley height (P-V) value for aluminium metal surface in the absence and presence of optimum concentration (2.0 g/L) of inhibitor is shown in Table 6. It is found that the values of Ra, Rq and P-V height is greater in alkaline solution without adding any inhibitor. This data suggested that AA surface has a greater surface roughness due to the dissolution of metal in alkaline solution but the values significantly reduced in the presence of 2.0 g/L ASB extracts in alkali solution. These parameters confirmed about smoother surface and the smoothness of the surface is due to the formation of a compact protective film of on the metal surface thereby inhibiting the corrosion of aluminium metal.

Table 7: AFM data for aluminium surface immersed in uninhibited and inhibited environments

Samples	RMS (Sq) roughness (nm)	Average (Sa) roughness (nm)	Area (St) peak-to-valley- height (nm)
Aluminium metal Immersed in 1 M NaOH solution	109.99	87.30	806.23
Metal immersed in 1 M NaOH containing ASB extract solution	20.64	15.27	157.19

3.4 Explanation for inhibition

The extract of ASB in this study contains various naturally occurring chemical compounds. The principal chemical constituent of the aqueous extract of leaves are given in Table 1.

It is generally assumed that aluminium has great affinity for ambient oxygen for the formation of protective oxide layer:

$$2Al_{(metal)} + 3/2\ O_{2\ (gas)} \leftrightarrow Al_2O_{3\ (solid)}$$

The oxide film formed act as a static barrier that isolate the metal from the solution. However, alkaline solutions may affect its properties. The dissolution of aluminium in alkaline solution is due to the following reaction:

$$Al + 3H_2O + OH^- \rightarrow 3/2\ H_2 + [Al\ (OH)_4]^-$$

The soluble complex ion formed leads to the dissolution of the metal. The adsorption of inhibitor molecules on metal surface is considered as a displacement reaction involving removal of H_2O molecules from the metal surface and adsorption of inhibitor molecules on metal surface [46] :

$$Inhibitor_{(sol)} + nH_2O_{(ads)} \leftrightarrow Inhibitor_{(ads)} + nH_2O_{(sol)}$$

The high inhibition efficiency shown by this extract is attributed to the presence of various organic compounds containing heteroatoms, -OH groups and pi bonds in the ASB extract (Table 1). The inhibitors adsorbed on the surface of aluminium and create a protective film on it. This restricts the diffusion of ions to or from the metal surface and hence retards the overall corrosion process.

The interactions of the adsorbed inhibitor molecules with the metal surface may prevent the metal atoms from participating in the anodic reaction of the corrosion. This simple blocking effect decreases the number of metal atoms participating and hence decreases the corrosion rate. [47].

Conclusion

Based on the results of investigation, the following conclusions are drawn:

1. ASB is a good eco-friendly green inhibitor for the corrosion control of aluminium in 1 M NaOH solution.
2. Inhibition efficiency of ASB extract increases with increasing concentration and decreases with rise in temperature.
4. The adsorption of inhibitor molecules on the surface of aluminium follows Langmuir adsorption isotherm.
5. Energy of activation value suggests that chemical present in ASB extract adsorbed chemically on the surface of aluminium.

Acknowledgement-Authors are highly thankful to Prof. V. B. Singh, Head (Department of chemistry), B.H.U. for providing SEM and AFM facilities for successful completion of my research work.

References

1. Wang L., Wan W., Yan G., Li D., Xua J., Wan H., Leun M. K. H., Li F., *Int. J. Hydrogen Energy*, 38 (2013) 14801.
2. Zhang J., Klasky M., Letellier B. C., *J. Nucl. Mater*. 384 (2009) 175.
3. Khaled K. F., *Corros Sci*. 52 (2010) 2905.
4. Quraishi M.A., Sardar R., *Corrosion* 58 (2002) 103.
5. Quraishi M.A., Sardar R., *Corrosion* 58 (2002) 748.
6. Eddib A., Hamdani M., *Mor. J. Chem.* 2 N°3 (2014) 165
7. Lebrini M., Lagrenee M., Vezin H., Gengembre L., Bentiss F., *Corros. Sci*. 47 (2005) 485.
8. Bentiss F., Bouanis M., Mernari B., Traisnel M., Vezin H., Lagrenee M., *Appl. Surf. Sci.* 253 (2007) 3696
9. Chikh Z. A., Chebabe D., Dharmraj A., Hajjaji N., Srhirri A., Montemor M.F., Ferreira M.G.S., Bastos A. C., *Corros. Sci*. 47 (2005) 447.
10. El-Etre A. Y, *Corros Sci*. 40 (1998) 1845.
11. El-Etre A. Y, *Corros Sci.* 45 (2003) 2485.
12. El-Etre A. Y. Abdallah, M., El-Tantawy Z. E., *Corros Sci*. 47 (2005) 385.
13. Pratap B., Chakraborthy G.S., Mogha N., *Int. J. Pharm. Tech. Research*, 5 (2013) 17.

14. Eddy N.O., Ebenso E.E., *Afr. J. Pure Appl. Chem*. 2 (2008) 46.
15. Salim A. A, Garson M. J., Craik D. J., *J. Nat. Prod*. 67 (2004) 1591.
16. Hui, T., Sun, Y., Zhu, L., Guo, W., Rao, G., *Zhongguo Zhong Yao Za Zhi*, 34 (2009) 1111.
17. Wang F., Ren F. C., Liu J. K., *Phytochemistry*, 70 (2009) 650.
18. Rastogi R. M., Mehrotra B. N., Central Drug Research Institute, Lucknow, India, 1990.
19. Rajic A., Kweifio-Okai G., Macrides T., Sandeman R. M., Chandler D. S., Polya, G. M., *Planta Medica*, 66 (2000) 206.
20. Chaubey N., Singh V. K., Savita Quraishi M. A., Ebenso E., E., *Int. J. Electrochem. Sci.*, 10 **(**2015**)** 504.
21. Martinez S., Stern I., Appl. *Surf. Sci.* 199 (2002) 83.
22. Yadav, D. K., Quraishi, M. A., *Ind. Eng. Chem. Res.* 51 (2012) 8194.
23. Majidi L., Faska Z., Znini M., Kharchouf S., Bouyanzer A., Hammouti B., *J. Mater. Environ. Sci.* 1 (2010) 219.
24. Tourabi M., Nohair K., Nyassi A., Hammouti B., Chetouani A., Bentiss F., *Mor. J. Chem*. 1 (2013) 33.
25. Tang L., Li X., Li L., Mu G., Liu G., *Mater. Chem. Phys*, 97 (2006) 301.
26. Tebbji K., Faska, N., Tounsi, A., Ouddad, H., Benkaddour, M., Hammouti, B., *Mater. Chem. Phys.* 106 (2007) 260.
27. Mu G., Li X., Liu G., *Corros Sci.* 47 (2005) 1932.
28. Outirite M., Lagrenee M., Lebrini M., Traisnel M., Jama C., Vezin H., Bentiss F., *Electrochim. Acta.* 55 (2010) 1670.
29. Ansari K. R., Quraishi M. A., *J. Ind. Eng.Chem*. 20 (2014) 2819.
30. Shao H. B., Wang J. M., Zhang Z., Zhang J. Q., Cao C. N., *Mater. Chem. Phys*. 77 (2003) 305.
31. Abdel-Gaber A. M., Khamis E., Abo-ElDahab Sh., Adeel H., *Mater. Chem. Phys.* 109 (2008) 297.
32. Kumari P .D. R., Nayak J., Shetty A. N., *Arab. J. Chem*. (2012) http://dx.doi.org/10.1016/j.arabjc.2011.12.003.
33. Mansfeld F., Lin S., Kim S., Shih H., *Corros. Sci*. 27 (1987) 997.
34. Brett C. M. A., *J. Appl. Electrochem.*, 20 (1990) 1000.
35. Brett C. M. A., *Corros Sci.* 33 (1992) 203.
36. Amin M. A., Abd EI-Rehim S. S., El-Sherbini E. E.F., Hazzazi O. A., Abbas M. N., *Corros Sci*.51 (2009) 658.
37. Emregu K. C., Aksut A. A., *Corros Sci*. 42 (2000) 2051.
38. Yadav D. K., Quraishi M. A., *Ind. Eng. Chem. Res*. 51 (2012)14966.
39. Khaled K. F., Amin M. A. *Corros. Sci.* 51 (2009) 1964.
40. Yadav D. K., Chauhan D. S., Ahamad I., Quraishi M. A., *RSC Advances*, 3 (2013) 632.
41. Ansari K. R., Quraishi M. A. Singh A., *Corros Sci.* 79 (2014) 5.
42. Ansari K. R., Sudheer, Singh A., Quraishi M. A., *J. Dispersion Sci. Technol*. DOI /10.1080/01932691.2014.938349.
43. Sangeetha M., Rajendran S., Sathiyabama J., Krishnaveni A., Shanthy P., Manimaran N., Shyamaladevi B., *Electrochim. Acta* 29 (2011) 429.
44. Rosliza R., Senin H.B., Wan Nik W.B., *Colloids Surf.* 312 (2008) 185.
45. Ansari K. R., Yadav D. K., Ebenso E. E., Quraishi M.A., *Int. J. Electrochem. Sci.* 7 (2012) 4780.
46. Hamdi A., Taouti M. B., Benbertal D., *J. Mater. Environ. Sci*., (2015) 93.
47. Prabhu D., Rao P., *J. Environ. Chem. Eng*. 1 (2013) 676.
48. Lee S. J., Cho S. A., An S. S., Na Y. J., Park N. H., Kim H. S., Lee C. W., Kim H. K., Kim E. K., Jang Y. P., Kim J. W., *Evidence-Based Complementary and Alternative Medicine*, 2012 (2012) 1.